Research Square

Preprints are preliminary reports that have not undergone peer review.
They should not be considered conclusive, used to inform clinical practice,
or referenced by the media as validated information.

The gut microbiota mediates triptolide-induced liver injury via the gut-liver axis

Yulin Wang
Shuguang Hospital, Shanghai University of Traditional Chinese Medicine
Yeqing Hu
Shuguang Hospital, Shanghai University of Traditional Chinese Medicine
Yuting Liu
Shuguang Hospital, Shanghai University of Traditional Chinese Medicine
Haibo Zhang
Shuguang Hospital, Shanghai University of Traditional Chinese Medicine
Xueying Liu
Shuguang Hospital, Shanghai University of Traditional Chinese Medicine
Hua Zhou
Shuguang Hospital, Shanghai University of Traditional Chinese Medicine
Chenghai Liu
Shuguang Hospital, Shanghai University of Traditional Chinese Medicine
Tao Yang (yangtao@shutcm.edu.cn)
Shuguang Hospital, Shanghai University of Traditional Chinese Medicine

Research Article

Keywords: triptolide, liver injury, gut microbiota, Reg3b, Reg3g, gut-liver axis

Posted Date: May 15th, 2023

DOI: https://doi.org/10.21203/rs.3.rs-2902171/v1

License: This work is licensed under a Creative Commons Attribution 4.0 International License.
Read Full License

Abstract

Triptolide (TP) is a toxic component of *Tripterygium wilfordii* Hook. f. that exhibits liver and gastrointestinal toxicity. However, TP-induced liver injury varies between individuals via an unknown mechanism, which limits the safe clinical application of TP. Herein, we aimed to study the mechanism underlying the regulation of TP-induced liver injury via the gut-liver axis using a multi-omics technique. C57BL/6 mice were administered with TP at 800 μg/kg. We also constructed a mouse model based on the male C57BL/6 gut microbiota with quadruple antibiotics. 16S rRNA gene sequencing, hematoxylin and eosin staining, and biochemical analyses were used to analyze the intestinal microbiota composition in stool samples and TP-induced hepatotoxicity and enterotoxicity. Proteomics and targeted metabonomics were performed to analyze key proteins related to intestinal injury and differential liver metabolic markers. Gut microbiota *Lactobacillus* and *Bacteroides* were related to TP hepatotoxicity, while the *Lactobacillus rhamnosus* or *Bacteroides fragilis* colonization alleviated TP-induced liver and ileum damage after gut microbiota disorder. Multi-omics analyses showed that the TP caused changes in genes related to intestinal and liver immune responses. Gut microbiota disorder amplified related immune responses, causing changes in intestinal immune barrier-related proteins REG3B and REG3G and changes to liver metabolites via the gut-liver axis. Thus, the gut microbiota (via the gut–liver axis) plays an important role in liver injury induced by TP, allowing a better interpretation of TP-induced hepatotoxicity.

Introduction

Tripterygium Wilfordii Hook. f. (TW) is a traditional Chinese medicine that is mainly used in the clinic in the form of tablets to treat rheumatoid arthritis, nephrotic syndrome, and lupus erythematosus (Li et al. 2014;Wang et al. 2017;Zhou et al. 2018). However, its therapeutic dose is close to the toxic dose, and there are increasing reports of clinical adverse reactions associated with its wide application(Fan et al. 2018;Hou et al. 2018). Triptolide (TP) is an epoxy diterpene lactone compound first extracted and isolated from TW in 1972 (Kupchan et al. 1972), and is one of the active components and main toxic components of TW. TP has disadvantages of low solubility, low bioavailability, narrow treatment window, and serious toxic and side effects, resulting in multiple organ toxicity, such as to the liver, kidney, heart, reproductive system, and gastrointestinal tract (Chen et al. 2021). Liver toxicity is the most serious side effect of TP. The differences in the TP content and toxicity in *TW* polyglycoside tablet preparations from different manufacturers were investigated, which showed that the TP content correlated positively with hepatocyte toxicity of TW polyglycoside tablet preparations (Wang et al. 2021). The characteristics of TP-induced liver injury are also difficult to predict and are irregular; moreover, its toxic mechanism is unclear (Yang et al. 2013).

Medical research on the gut microbiota shows that individual differences in the composition of the human gut microbiota will lead to differences in drug reactions. When taken orally, a drug inevitably enters the gastrointestinal tract and interacts with the gut microbiota (Carmody and Turnbaugh 2014;Koppel et al. 2017). Drugs can change the composition and function of the gut microbiota, and in turn, the gut microbiota can affect the chemical transformation a drug (Clarke et al. 2019). The gut

microbiota and drugs interact directly or indirectly with each other. On the one hand, changes to the gut microbiota can cause changes to gut microbial metabolites, for instance, it can synthesize and release a large group of metabolites, such as short-chain fatty acids (SCFAs), choline metabolites, and lipids (Nicholson et al. 2012;Kalantar-Zadeh et al. 2019). Some gut microbial metabolites can affect host drug transporters liver drug enzymes, and other reactions of the body, resulting in changes to the efficacy and toxicity of drugs. For example, SCFAs can regulate the host's immune system (Feng et al. 2018). On the other hand, the gut microbiota can directly metabolize drugs (Zimmermann et al. 2019). Drugs entering the intestine undergo a change in compound structure through biotransformation by the symbiotic gut microbiota, causing changes in drug efficacy and its therapeutic effect (Koppel et al. 2017). For example, drugs and glucuronic acid can be combined through the intestinal bacteria β-Glucuronidase to inactivate and detoxify drugs, thereby reversing glucuronidation-mediated druginduced gastrointestinal toxicity (Wallace et al. 2015). In conclusion, the drug response varies considerably between different individuals, and the efficacy and toxicity of drugs are highly affected by the gut microbiota (Lam et al. 2019).

TP and the gut microbiota can interact. On the one hand, TP has antibacterial activity *in vitro*. It can inhibit 48 kinds of bacteria, such as *Staphylococcus aureus* and gram-negative bacteria (Wang and Hu 2010). A study showed that TP can also inhibit the growth of intestinal Firmicutes and improve ulcerative colitis (Wu et al. 2020). On the other hand, the gut microbiota affects TP hepatotoxicity. Studies have shown that antibiotic intervention can increase the liver toxicity of intraperitoneal injection of TP after intestinal flora disorder, and its mechanism is related to propionic acid, a metabolite derived from the gut microbiota (Huang et al. 2020). In conclusion, gut microbiota and TP can interact with each other; however, the mechanism by which the gut microbiota affect TP-induced hepatotoxicity is unknown.

The liver and gut are closely connected through the gut-liver axis. They form a two-way connection through the portal vein system and systemic circulation for close communication. When the intestinal barrier is damaged, microorganisms and their derivatives transfer to the liver through the portal vein, which aggravates liver injury (Seki and Schnabl 2012). Some displaced intestinal products can also interact directly with the host, resulting in the deterioration of liver disease (Filliol et al. 2017). Studies have found the use of antibiotics (Tulstrup et al. 2015) will lead to intestinal inflammation and microbiota imbalance(Henao-Mejia1 et al. 2012), which is also the main driving factor for the increase of intestinal permeability. Our previous study found that after antibiotic pretreatment, the hepatotoxicity, blood concentration, and bioavailability of TP were increased, suggesting that TP hepatotoxicity was closely related to gut microbiota (Liu et al. 2022).

In conclusion, TP-induced liver injury and the hepatotoxicity of TP are closely related to the gut microbiota. Most previous studies were limited to the direct mechanism of TP-induced hepatotoxicity; however, its mechanism remains unclear. The present study focused on the gut microbiota and analyzed the mechanism of TPinduced liver injury from the perspective of the gut-liver axis.

Materials and methods

Reagents and preparation

Triptolide (T34030F3D) was purchased from Shanghai Acmec Biochemical Co., Ltd) (Shanghai, China), Vancomycin (H13M11Y113102), Metronidazole (B08O10E99250), Ampicillin (Z12A11X111028) and Neomycin (S20S10Y98095) were all from Shanghai Yuanye Biotechnology Co., Ltd (Shanghai, China). The antiF4/80 antibody (70076T) was purchased from Merck KGaA (Darmstadt, Germany). The anti-NLRP3 antibody (337DDA21) was purchased from Thermo Fisher Scientific (Waltham, MA, USA). QuickBlock™ Secondary Antibody Dilution Buffer (P0267) was obtained from Beyotime Biotechnology Co., Ltd (Shanghai, China). The Stool Genomic DNA Extraction Kit (M4015-02) was from Omega Biotek (Norcross, GA, USA). The Qubit™ dsDNA HS Assay Kit (Q32851) was from Thermo Fisher Scientific. *Bacteroides fragilis* (ATCC 25285) and *Lactobacillus rhamnosus* (ATCC 53103) were obtained from Ningbo Taisituo Biotechnology Co., Ltd. (Zhejiang, China). The TMTsixplex™ Label Reagent (WD319469) was obtained from Thermo Fisher Scientific. The Q300 Metabolic Chip Test Kit (HY5023R) was supplied by MetaboProfile Biotechnology Co., Ltd. (Shanghai, China). Anti-REG3G antibodies (ab198216) were purchased from Abcam (Cambridge, UK).

An appropriate amount of TP was accurately weighed, add an appropriate amount of ethanol solution used to dissolve it, after which it was dispersed in ultrapure water (the final concentration of ethanol is 3%), so that the final concentration of TP was 80 μg/mL. The *Bacteroides fragilis* and *Lactobacillus rhamnosus* preserved in glycerin were revived and activated using the plate coating method. After anaerobic culture, they were subcultured, collected, and gradient diluted. Finally, the corresponding multiple after plate coating culture again was diluted to make the concentration of the target bacterial solution 10^8 CFU/mL.

Animals and treatment

Male C57BL/6 mice (22 ± 2 g) were purchased from Beijing Vital River Laboratory Animal Technology Co., Ltd (Beijing, China), and raised in the experimental animal center of Shanghai University of traditional Chinese medicine. Mice were maintained in an environment with a temperature of 20–26 ℃, a humidity of 40–70%, and a standard 12 h light/dark cycle (6:00 am – 6:00 pm). Mice ate and drink freely. Mice were divided into four groups to collect feces, blood samples, and liver tissues after gas anesthesia: Male C57BL/6 mice were raised in Specific Pathogen-Free (SPF) and clean laboratory (CL) environments, respectively. Mice in the SPF and CL environments were randomly divided into two groups: The control group (CON) and the triptolide group (TP), with 10 mice in each group. The groups comprised SPF-CON group (SPF-CON-B before gavage, SPF-CON-A after gavage), SPF-TP group (SPF-TP-B before administration; SPF-TP-A after administration), CL-CON group (CL-CON-B before administration; CL-CON-A after administration) and CL-TP group (CL-TP-B before administration; CL-TP-A after administration).

Mice were divided into six groups to collect blood samples, liver and ileum tissues: Control group (3% ethanol solution), TP group (triptolide solution 800 μg/kg dissolved in 3% ethanol solution, once a day for 1 day), ABx group (treated with an antibiotic cocktail comprising four antibiotics, vancomycin 50 mg/kg, neomycin 100 mg/kg, metronidazole 100 mg/kg, and ampicillin 100 mg/kg, once a day for 7 days), ABx

+ TP group (after 7 days of administration of antibiotic cocktail, triptolide solution was administered by gavage on the 9th day at an interval of one day in order to eliminate drug interactions), LGG (2×10^8 CFU of *Lactobacillus rhamnosus* for 4 weeks) + TP (administration of triptolide solution 800 μg/kg on the 29th day) group, BF (2×10^8 CFU of *Bacteroides fragilis* for 4 weeks) + TP (administration of triptolide solution 800 μg/kg on the 29th day) group (Liu et al. 2019) .(Fig. 1)

Histological analysis

The liver and ileum tissues were washed with phosphate buffered saline (PBS) and fixed in 10% formalin solution for more than 24 h. After dehydration, the tissues were embedded in paraffin and sliced into 4–6 pieces, stained with hematoxylin and eosin (H&E), and photographed under an optical microscope.

Serum aminotransferase assays

Blood samples were collected and centrifuged at 3, 500 rpm·min^{-1}, 4°C for 10 min to obtain supernatants for alanine aminotransferase (ALT), aspartate aminotransferase (AST), and albumin (ALB) analysis. The level of ALT, AST, and ALB were tested using available kits (Nanjing Jiancheng Bioengineering Institute, China) according to the manufacturer's instructions.

Immunocytochemistry analysis

The paraffin embedded liver or ileum tissue sections were dewaxed and washed with water and PBS for 3 times/5 min. respectively. After microwave antigen repair with citric acid, 3% H_2O_2 was added and incubated for 15 min at 37°C washed with PBS for 15 min, then serum blocking solution was added dropwise for 10 min at 37°C. Next, 30 μL of F4/80 antibody, NLRP3 antibody, or REG3G antibody added and incubated overnight at 4 ℃, and then washed with PBS for 3 times/5 min. QuickBlock™ secondary antibody buffer was added and incubated at 37 ℃ for 30 min, washed with PBS 3 times/5 min, and then dehydrated, made transparent, sealed, and then subjected to microscopic examination after color development.

16 S rRNA sequencing of fecal microbiota

Fecal samples were taken for DNA extraction and PCR amplification. Total fecal DNA was extracted using the E.Z.N.A®. Mag-Bind® Stool DNA Kit (M4015-02, Omega Biotek). The V3–V4 regions of the 16S rRNA gene were amplified by PCR with the bacterial primers 341F (5 '-CCTACGGNGGCWGCAG-3') and 806R (5'-GGA CTA CHV GGG TWT CTAAT-3'). The Qubit™ dsDNA HS kit and qubit fluorometer were used to detect the concentration of samples. The library was sequenced according to the Miseq standard operating procedures (Illumina, San Diego, CA, USA). The cluster approach of Quantitative Insights into Microbial Ecology (QIIME) (V1.9.1) was used to process the 16S recombinant DNA sequencing data, from which the useful Tags were acquired(Caporaso et al. 2020). UPARSE (V9.2.64_i86linux32) software was used to divide the OTUs according to the 97% similarity threshold standard and used similarity as the division basis to turn the most effective data into OTUs (Edgar 2013). The species were annotated using Greenenes (gg_13_5), and the threshold of the degree of confidence was set to 0.8-1(Desantis et al. 2006). Mothur (V.1.30) software was used to examine the rarefaction curve and Shannon index to reflect

the alpha diversity of the samples. The Bray–Curtis algorithm of QIIME and the R software were used to assess the similarities of species diversity in various datasets to reflect their beta diversity. Finally, ANOVA analysis was carried out to screen species with significant genus-level differences ($P < 0.05$).

Protein extraction

SDT (4% SDS, 100 mM Tris-HCl, 1. mM DTT, pH 7.6) buffer was used for sample lysis and protein extraction. The amount of protein was quantified using a bicinchoninic acid (BCA) Protein Assay Kit (Bio-Rad, Hercules, CA, USA). Protein digestion by trypsin was performed according to filter-aided sample preparation (FASP) procedure described by Matthias Mann(Wiśniewski et al. 2009). The digested peptides of each sample were desalted on a C18 Cartridges (Empore™ SPE Cartridges C18 (standard density), bed I.D. 7 mm, volume 3 mL, Sigma, St. Louis, MO, USA), concentrated by vacuum centrifugation, and reconstituted in 40 µL of 0.1% (v/v) formic acid. Then, 20 µg of protein for each sample were mixed with 5· loading buffer and boiled for 5 min. The proteins were separated on a 12.5% SDS-PAGE gel (constant current 14 mA, 90 min). Protein bands were visualized by Coomassie Blue R-250 staining. Then, 100 µg peptide mixture of each sample was labeled using the Tandem Mass Tag (TMT) reagent according to the manufacturer's instructions.

Liquid chromatography tandem mass spectroscopy (LC-MS/MS) analysis of proteins

LC-MS/MS analysis was performed on a Q Exactive mass spectrometer (Thermo Scientific) that was coupled to an Easy nLC (Proxeon Biosystems, now Thermo Fisher Scientific) for 60 min. The peptides were loaded onto a reverse phase trap column (Thermo Scientific Acclaim PepMap100, 100 µm*2 cm, nanoViper C18) connected to the C18-reversed phase analytical column (Thermo Scientific Easy Column, 10 cm long, 75 µm inner diameter, 3µm resin) in buffer A (0.1% Formic acid) and separated with a linear gradient of buffer B (84% acetonitrile and 0.1% Formic acid) at a flow rate of 300 nL/min controlled by IntelliFlow technology. The mass spectrometer was operated in positive ion mode. MS data were acquired using a data-dependent top10 method dynamically choosing the most abundant precursor ions from the survey scan (300–1800 m/z) for Higher-energy C-trap dissociation (HCD) fragmentation. The automatic gain control (AGC) target was set to $3e^6$, and maximum injection time to 10 ms. Dynamic exclusion duration was 40.0 s. Survey scans were acquired at a resolution of 70,000 at m/z 200 and resolution for HCD spectra was set to 17,500 at m/z 200, and isolation width was 2 m/z. Normalized collision energy was 30 eV and the underfill ratio, which specifies the minimum percentage of the target value likely to be reached at maximum fill time, was defined as 0.1%. The instrument was run with peptide recognition mode enabled. The MS raw data for each sample were searched using the MASCOT engine (Matrix Science, London, UK; version 2.2) embedded into Proteome Discoverer 1.4 software for identification and quantitation analysis.

Pathway analysis

The differentially abundant proteins were locally searched using the NCBI BLAST + client software (ncbi-blast-2.2.28+-win32.exe) and InterProScan to find homologous sequences, then GO terms were mapped,

and sequences were annotated using the software program Blast2GO (https://www.blast2go.com/). The GO annotation results were plotted using R scripts. The online KEGG database (http://geneontology.org/) was used to retrieve their KEGG orthology identifications and were subsequently mapped to pathways in KEGG.

Metabolite extraction and separation

Liver tissue (10 mg) was weighted, and deionized water, magnetic beads, and precooled methanol solution (including 120 μL of internal standard working solution) were added. The mixture was homogenized at 4 ℃ for 3 min a speed 8, followed by centrifugation at 18, 000 · *g* at 4°C for 20 min to obtain liver tissue extract solutions. Then, 20 μL of liver tissue extracts were added to a 96-well plate, and 20 μL of derivatization reagent and 20 μL of EDC working solution were added. The plate was sealed, incubated at 30°C for 5 min, and then centrifuged at 4, 000 · *g* for 30 min at 4 ℃to obtain the supernatant. Next, 10 μL of IS II working solution was added to a new 96-well plate with 140 μL of the supernatant. The plate was centrifugated at 650 rpm for 5 min. Finally, the plate was sealed for LC-MS analysis. A Waters ACQUITY UPLC-Xevo TQ-S with an ESI source was used for metabolite analyses (Waters, Milford, MA, USA). Chromatographic separation was performed using a C18 column (1.7 μm, 2.1×100 mm) (Waters) at a flow rate of 0.4 mL·min^{-1}. Chromatographic separations were performed on an ACQUITY BEH C18 column (1.7 μm, 100 mm × 2.1 mm internal dimensions) (Waters) maintained at 40°C.

Mobile phase A was 0.1% formic acid water, and mobile phase B was acetonitrile. The gradient elution conditions were as follows: 0–1 min, 5% B; 5 min, 30% B; 9 min, 50% B; 11 min, 78% B; 13.5 min, 95% B; 14–16 min, 100% B; 16.1 min, 5% B; 18 min, 5% B. The mass spectrum was analyzed using an electrospray spray ion source (ESI), which scans in the positive and negative ion mode. The capillary voltage was + 1.5 / − 2.0 kV, the ion source temperature was 150 ° C, the desolvent temperature was 550 ° C, and the desolvent gas flow is 1000 L/hr.

Differential Metabolites Selection

The original data was processed by Mass Lynx software (V 4.1), and all samples are subject to noise reduction, baseline correction, peak identification, peak alignment, peak extraction, and normalization. The metabolites were quantified using the standard curve method, and statistical analysis is conducted using the iMAP (V 1.0) platform. Principal component analysis was used to investigate the overall metabolic distribution among the samples of each group. PLS-DA was used to identify the main difference variables that caused such aggregation and dispersion. OPLS-DA was used to further identify and differentiate the metabolites that contributed significantly to the metabolic profile among the groups. The multi-dimensional statistical results were verified using a univariate statistics method. VIP > 1.0 and $P < 0.05$ were used as screening criteria, to find potential biomarkers that might play critical roles in biological processes related to the study by obtaining the intersection of the differential metabolites from univariate statistics and multi-dimensional statistics.

Statistical analysis

SPSS 26.0 (IBM Corp., Armonk, NY, USA) was used for the statistical analysis, and data conforming to normal distribution and homogeneity of variance were expressed by the mean ± SD. Single factor analysis of variance (ANOVA) was used for comparison between groups, and the least significant difference (LSD) method was used for comparisons between two samples. The measurement data that did not conform to the normal distribution or the uneven variance are expressed by the median and interquartile interval [Medium (IQR)]. Mann Whitney U-rank sum test was used for comparison between two groups, and the Kruskal–Wallis H-rank sum test was used for comparisons among multiple groups. Statistical significance was accepted if $\alpha = 0.05$, and the *P*-values were < 0.05.

Results

Differences in liver injury after the administration of TP in SPF and CL environments

The schematic diagram of the animal grouping is shown in Fig. 1. The mice were from the same vendor, and they were raised in specific pathogen free (SPF) and clean laboratory (CL) environments, respectively. After administration of TP at 800 μg/kg·d^{-1}, the appearance of liver; serum alanine transaminase (ALT), aspartate transaminase (AST) and albumin (ALB) levels; and histological analysis were used to assess liver toxicity. The state of the mice showed that mice raised in the SPF environment moved slowly and even died after TP administration. The hematoxylin and eosin (H&E) staining showed severe pathological changes, including extravasated blood, and severe destruction of the cell structure of the liver (Fig. 2A). However, mice raised in the CL environment were still active after the administration of TP, and the pathological sections of the liver showed no significant damage. Likewise, the ALT and AST levels of the SPF-TP group were significantly higher than those of the CL-TP group, whereas the ALB levels were significantly decreased ($P < 0.01$). In addition, the ALT and AST levels of the SPF-TP and CL-TP groups were significantly higher than those of their respective controls (SPF-CON and CL-CON), respectively ($P < 0.01$) (Fig. 2B).

OTU analysis and species annotation of the gut microbiota

After filtering, noise reduction, splicing, and removal of chimeras from the 16 S rRNA sequencing data, a total of 6745 operational taxonomic units (OTUs) were generated from 74 samples, and an average of 91 OTU sequences were generated from each sample. In all samples, the length of the generated sequences was 150–292 bp, with an average length of 282 bp. According to the abundance of the OTUs, Venn diagrams were drawn to interpret the differences in OTUs among the different groups (Fig. 3A). The Venn diagram showed that there were fewer OTUs in the mice from the SPF environment after administration of TP than that before administration, and the OTUs of the mice from the SPF environment were significantly different from those in the mice from the CL environment before and after TP administration. Combining the species annotation information of OTUs and the numbers of OTUs in different samples, the expression of each sample at each taxonomic level was counted according to kingdom > phylum > class > order > family > genus > species (Fig. 3B). According to the definition that a

phyla with a relative abundance of more than 50% in any sample is the main phyla, the main phyla was identified as Firmicutes (74.41%) for all samples. Phyla with a relative abundance > 5% outside the main phylum were defined as the secondary phyla, which in all samples mainly included four phyla: Bacteroidetes (19.53%), Actinomycetes (4.05%), Verrucomicrobiota (0.94%), and Desulfobacteria (0.35%). The genera detected in 90% of the samples included *Lactobacillus*, *Muribaculaceae*, *Enterorhabdus*, *Clostridia_UCG-014*, *Lachnospiraceae_NK4A136_group*, *Lachnoclostridium*, *[Eubacterium]_xylanophilum_group*, *Streptococcus*, *[Eubacterium]_coprostanoligenes_group*, *Blautia*, *RF39*, *Incertae_Sedis*, *[Eubacterium]_brachy_grou*p, *[Eubacterium]_nodatum_group*, *Anaerotruncus*, and *Lachnospiraceae_UCG-006*, *UCG-010* (Fig. 3C).

Changes in alpha and beta diversity of the gut microbiota before and after TP administration in the SPF and CL environments

The Shannon rarefaction curve can reflect the abundance of species in samples. The results showed that the curve tended to be flat, and it is believed that the increase of sequencing depth did not affect the diversity of species, and the sequencing volume was sufficient (Fig. 3D). The Shannon index before and after administration of TP was calculated for mice in the SPF and CL environments, and the differences in microbial Alpha diversity were analyzed using Tukey's test and the Kruskal–Wallis rank-sum test. In the SPF environment, compared with before and after the administration of TP, the Alpha diversity of SPF-TP-A (after TP; median Shannon index = 7.34) was higher than that of SPF-TP-B (before TP; median Shannon = 6.75). In the CL environment, compared with CL-TP-B (before TP; Shannon median = 5.98), the alpha diversity of SPF-TP-B (Shannon median = 6.75) was higher. The boxplots of Shannon's index for each comparison group are shown in Fig. 3E. Comparing the Shannon index between CL-TP-A (after TP; Shannon median = 6.24) and SPF-TP-A (Shannon median = 7.34), there was a significant difference between the two groups ($P \leq 0.01$); moreover, the alpha diversity of CL-TP-B (Shannon median = 5.98) was higher than that of CL-TP-A (Shannon median = 6.24) (Fig. 3E). The results of Shannon indexes showed that TP exposure decreased the alpha–diversity. Among β diversity analyses, ANOSIM analysis is often regarded as a quantitative value to reflect the difference in community species composition among samples in each group. The distance boxplot of each comparison group showed that compared with the SPF environment, the R value after TP administration in the CL environment was 0.89, and the R value was 0.486 before administration in the CL environment, which were significantly different ($P = 0.001$). The R value was 0.175 ($P = 0.001$) before and after administration of TP under the SPF environment, and the R value is 0.180 ($P = 0.007$) before and after administration of TP under the CL environment (Fig. 3F). These results indicated that the differences in the bacterial community structure between the CL environment and the SPF environment were significant, and the differences in the bacterial community structure before and after the administration of TP in the SPF environment were more significant than those in the CL environment before and after the administration of TP.

Differences of the composition of the gut microbiota before and after TP administration in the SPF and CL environments

To further clarify the global differences in bacterial composition between the mice before and after administration in the SPF and CL environment, species differences was performed. Linear discriminant analysis effect Size (LEfse) software was used to analyze species differences between groups, and we used a mapping evolutionary branch diagram to display and rank the differences in microbial community abundance. There were 49 genera with statistically significant differences between the SPF-TP-A group and the CL-TP-A group. Among them, genera with a relative abundance greater than 1%, including *Lachnoclostridiu*, *[Eubacterium]_xylanophilum_group*, *[Eubacterium]_coprostanoligenes_group*, *Brautia*, *Muribaculaceae*, *Lachnospiraceae_NK4A136_group* increased in the SPF-TP-A group, and *Bacteroidetes* and *Lactobacillus* decreased in SPF-TP-A group compared with the CL-TP-A group (Fig. 3G, H). A total of 51 genera showed statistically significant differences between the SPF-TP-B group and the CL-TP-B group before administration of TP, among the genera with relative abundance greater than 1%, *Blautia*, *[Eubacterium]_xylanophilum_group*, *Lachnospiraceae_NK4A136_group*, *Lachnoclostridium* and *Muribaculaceae* increased in the SPF-TP-B group, and *Bacteroides*, *Alistipes* and *Lactobacillus* decreased in the SPF-TP-B group compared with the CL-TP-B group (Fig. 3G, H). Taken together, the results indicated that *Bacteroides* and *Lactobacillus* are closely related to the liver injury induced by TP.

Gut microbiota disturbance induced by TP causes ileal injury and exaggerates liver injury in mice

We next sought to confirm the effect of gut microbiota on the toxicity of TP in mice through a gut microbiota disturbance model. We found that the administration of TP after disrupting the gut microbiota of mice with ABx (treatment with an antibiotic cocktail comprising four antibiotics: vancomycin 50 mg/kg, neomycin 100 mg/kg, metronidazole 100 mg/kg, and ampicillin 100 mg/kg, once a day for 7 days) resulted in more severe liver damage in mice, and significant damage to the ileum. The liver in the CON group had normal morphology, soft texture, a smooth surface, uniform color, light reddish-brown, and no lesions. The appearance of the liver in the ABx group was not significantly different from that in the CON group, and the liver cells were structurally complete and neatly arranged. The livers of the mice in the TP group were darker in color than those in the CON group. The livers were congested, the surface was granular, the cells were of different sizes, loosely arranged, and the nuclei were large and darkly stained, accompanied by inflammatory cell infiltration. The liver in the ABx + TP group had the darkest appearance, dark reddish-brown, severe congestion, uneven surface, disordered cell arrangement, increased mitosis, enlarged portal area with bridging necrosis, and large-scale cell necrosis, and the damage was the most serious. The liver appearance and H&E staining results of LGG (2×10^8 colony forming units (CFU) of *Lactobacillus rhamnosus* for 4 weeks) + TP group and BF (2×10^8 CFU of *Bacteroides fragilis* for 4 weeks) + TP group were similar to those of the TP group, but the degree of damage was slightly less than that of TP group, and the degree of liver damage in the LGG + TP group was lighter than that in the BF + TP group (Fig. 4A, B). Consistently, the serum levels of ALT and AST in the ABx + TP group were higher than those in the other groups. After colonization with LGG and BF strains, the levels of ALT and AST decreased (Fig. 4C). A study showed that there is also a tight connection between changes in the intestinal microecology and illnesses that are related to the intestines

(Zhua et al. 2021). Therefore, this also led us to further investigate whether TP causes intestinal damage after gut microbiota disorder. Therefore, we analyzed the damage degree of the ileum tissue by H&E staining. The results showed that the ileum tissue structure of the CON group was complete, the villi were neatly arranged, and there was no related inflammatory cell infiltration. The ABx and TP groups had mild inflammatory cell infiltration and villus breakage, the crypts were deformed and shortened, and the number of cells in the mucosal layer was decreased. The ileum tissue in the ABx + TP group was disorderly arranged, the crypts were shortened or even lost, the villi had fallen off, inflammatory cells were infiltrated, and the damage was severe. The ileum tissue of LGG + TP group and BF + TP group were similar and were damaged, in which the villi were arranged neatly, but were sparser and shorter, the crypts were reduced, and the spacing was slightly larger. The overall situation resembled to that of the TP group (Fig. 4D). These results indicated that gut microbiota plays a crucial role in the toxicity of TP.

Comprehensive Proteogenomic Characterization of the CON group and the ABx + TP group Samples

Ileum tissue samples from mice in CON group and the ABx + TP group were used for quantitative proteomic analysis. Quality control results are shown in Figures S1A-C. There were 272 significantly differentially abundant proteins between the two groups according to the screening criteria: foldchange (FC) (upregulation > 1.2, or downregulation < 0.83) and $P < 0.05$ (T-test). Compared with the CON group, 98 proteins in the ABx + TP group were downregulated, and 174 proteins were upregulated (Fig. 4E). The differentially abundant proteins are displayed in the form of a volcano map, and the significantly decreased proteins (FC < 0.83 and $P < 0.05$) are shown in blue, including dual oxidase maturation factor 2, regenerating islet-derived protein 3-gamma, coiled-coil domain-containing protein 88B, fermitin family homolog 3, and upstream stimulatory factor 1. Significantly upregulated proteins are marked in red (FC > 1.2 and $P < 0.05$), including cystathionine gamma-lyase, retinal dehydrogenase 1, metallothionein-2, and cytochrome c oxidase subunit 1 (Fig. 4F). Kyoto Encyclopedia of Genes and Genomes (KEGG) and gene ontology (GO) functional prediction analysis of the differentially abundant proteins were performed. The results showed that the differentially abundant proteins were mainly related to monocarboxylic acid metabolic process, oxidoreductase activity, retinol metabolism, linoleic acid metabolism, and drug metabolism - cytochrome P450 (Fig. 4G, H). The enrichment of GO entries under the three categories of GO biological process, molecular function and cellular component was displayed with a bubble chart and shown in Figures S2A-D. For more detailed KEGG analysis, see Figures S3A, B.

Intestinal immune barrier proteins REG3B and REG3G showed significant changes after TP administration in mice with a gut microbiota disorder

The intestinal barrier mainly comprises a microbial barrier, a chemical barrier, a physical barrier, and an immune barrier. These barriers play a major role in maintaining the stability of the internal and external environments ession of F4/80 in the ABx + TP group was significantly reduced in comparison with that in the CON or the ABx group. The ABx + TP group had the lowest positive expression of F4/80, which suggested that the number of Kupffer cells decreased after TP-induced liver injury, which was further

aggravated after the gut microbiota disturbance (Fig. 5C). These results indicated that gut microbiota disorder might affect the inflammatory reaction to TP in the liver through the gut-liver axis, thereby aggravating the liver injury caused by TP.

Liver biomarkers of gut microbiota aggravate TP hepatotoxicity via the gut-liver axis

In the liver metabolic profiling, principal component analysis (PCA) showed that the CON group and ABx + TP group could be clearly separated, and there were significant differences between the two groups. Next, we built partial least squaresdiscriminant analysis (PLS-DA) and orthogonal projections to latent structures discriminant analysis (OPLS-DA) models to verify the constructed model and showed that the two groups were obviously separated. Besides, a total of 111 differential metabolites between the two groups were identified through one-dimensional statistical analysis (Fig. 5D). One-dimensional analysis was screened using $P < 0.05$, $|\log2FC| \geq 0$, the multi-dimensional analysis results were screened with a variable importance in projection (VIP) > 1, and the potential biomarkers were obtained through the intersected multidimensional and single-dimensional screening results. These metabolites were mainly involved in tricarboxylic acid (TCA), taurodeoxycholic acid (TDCA), chenodeoxycholic acid (CDCA), dichloroacetate (DCA), hydroxycitric acid (HCA), butyric acid, asparagine, phenylalanine, isoleucine, leucine, tryptophan, and proline metabolism, which are closely related to liver injury or the immune system and are biomarkers of TP aggravation of liver injury after gut microbiota disorder. (Fig. 5E). The Heat map and Z Score plot of potential biomarkers are shown in Figures S4A, B. Boxplot of 11 differential metabolites are shown in Figure S5.

Discussion

Although TP hepatotoxicity is substantial, most studies have only focused on the direct mechanism of its hepatotoxicity; however, this mechanism is still unknown. To investigate the mechanism of TP-induced liver damage, this study focused on TP hepatotoxicity from the viewpoint of the gut-liver axis, in which process, the gut microbiota plays vital role.

Microbes colonizing the digestive tract have important functions in human health and disease, and have profound effects on the intestines, liver, pancreas, heart, and brain (Ho et al. 2015). Among them, the liver is close to the intestines and can be exposed to many bacteria and metabolites. The microorganisms and metabolites in the intestine pass through the intestinal barrier and the portal vein circulation and are then transported to the liver, thereby affecting liver physiology (Ho et al. 2015). The physiological changes and status of the liver are closely related to the changes in the gut microbiota (Tilg et al. 2016). The association of gut microbiota with TP hepatotoxicity was fully demonstrated in the present study. The gut microbiota was analyzed in mouse fecal samples before and after TP administration by DNA sequencing technology. The results showed that there was little difference in the gut microbiota and liver injury of CL mice before and after the administration of TP. In the SPF environment, there was no significant difference in the gut microbiota of the CON group before and after administration of the

control solvent. However, the gut microbiota showed obvious changes after TP administration. The proportion of *Bacteroidetes* increased after TP administration, however, the difference was small, and we speculated that it might have been caused by a short interval between the administration of TP and the collection of feces. The effect of the gut microbiota on TP hepatotoxicity was obvious. Mice in SPF environment had obvious liver damage after administration of TP, and it was more serious than that in mice in the CL environment. Our results showed that *Bacteroides* and *Lactobacillus* were less abundant in the SPF group; therefore, we speculated that they were associated with TP-induced liver injury. Studies have also shown that the genera *Bacteroides* and *Lactobacillus* are probiotics and are related to liver damage. *Lactobacillus rhamnosus* is useful in the prevention or treatment of various liver diseases, such as alcoholic liver disease and non-alcoholic liver disease (Wang et al. 2013;Mantegazza et al. 2018). Another study showed that LGG can reduce liver fibrosis in rodents with chronic liver disease (Ren et al. 2019). LGG was also beneficial in reducing bile acid accumulation and liver injury associated with intrahepatic cholestasis of pregnancy and improving liver injury and hypoxic hepatitis in cecal ligation and puncture-induced septic rats (Ding et al. 2019). *Lactobacillus* has also been shown to improve liver damage. A gut microbiota rich in *Lactobacillus* can induce the production of IL-22 by ILC3, thereby enhancing the intestinal mucosal barrier function and restoring the integrity of the intestinal epithelium, thus preventing the further transfer of intestinal derivatives and related factors to the liver to trigger hepatic inflammation (Nakamoto et al. 2017). Intervention with *L. salivarius LI01* could alter the microbial community, reduce the abundance of pathogenic microbial taxa, and enrich the abundance of beneficial flora, thereby restoring gut barrier biomarkers (Claudin-1 and MUC2), upregulating hepatic antiinflammatory cytokines (IL-10 and Toll-like receptor TLR-3), and attenuating acute liver injury induced by D-galactosamine injection in SD rats (Zhuge et al. 2020). These previous studies indicated that *Bacteroides* and *Lactobacillus* play an important role in liver injury, which also coincides with our experimental results. Except for *Bacteroides* and *Lactobacillus*, the proportion of *Blautia* before and after TP administration was consistently higher in the SPF group than in the CL group. *Blautia*, a commensal obligate anaerobic bacterium can be increased in children with non-alcoholic fatty liver disease(NAFLD)/non-alcoholic steatohepatitis (NASH) (Zhuge et al. 2020). However, *Blautia* can also upregulate intestinal regulatory T cells and produce SCFAs, which play an important role in maintaining the balance of the intestinal environment and preventing inflammation (Kim and Park 2014). Therefore, the relationship between *Blautia* and TP intestinal injury and liver injury should be further explored.

The gut microbiota is an important indicator of different states of the body. Various types of flora are opposed to each other, are interdependent, and involved in the movement and change of the "Yang and Yin" balance theory in traditional Chinese medicine. The constant changes in the internal and external environment, and the differences in the host will lead to changes in the quantity, type, and distribution of the gut microbiota. These changes will be reflected in the body’s response to the toxicity of traditional Chinese medicine above a certain level (Ni and Zhang 2009). Antibiotics can greatly affect the composition of the gut microbiota, reduce the biodiversity of the host, and lead to an imbalance of the microbiota (Angelucci et al. 2019). Therefore, the use of combined antibiotic intervention to construct a pseudo-germ-free mouse model is widely used in the study of gut microbiota and diseases, as well as

drug efficacy and toxicity, because of its convenience, economy, and availability. The quadruple antibiotic combination of vancomycin combined with metronidazole, neomycin sulfate, and ampicillin is a common antibiotic combination that depletes the gut microbiota of mice (Liu et al. 2019). Another study showed that there is also a close relationship between changes in the gut microecological environment and gut-related diseases (Zhua et al. 2021), which led us to speculate whether TP can cause gut damage after gut microbiota disturbance. Germ-free mice (GF) and antibiotic-induced gut microflora dysbiosis pseudo-germ-free mice are two common animal models used to study the relationship between the gut microbiota and disease. GF mice have been used in animal experiments since Pleasants successfully bred the first GF mouse in 1959 (Pleasants 1959). The use of GF animals has greatly promoted advances in research into intestinal microbiota and human-related diseases, providing a valuable experimental tool to study the interaction between the host and its microbiota (Arvidsson et al. 2012). However, due to the high cost and harsh experimental conditions used to create a GF model, the pseudo-germ-free mouse model constructed using oral antibiotics has been increasingly used in research into the intestinal flora and diseases, drug efficacy, and toxicity. Oral antibiotics can change and reduce the number and diversity of intestinal microorganisms, which is a common method to cause an imbalance of the gut microbiota (Wostmann et al. 1983). Different antibiotics have different effects on the intestinal flora. For example, vancomycin mainly acts on gram-positive bacteria (Uribe-Herranz et al. 2020), which can significantly reduce *Clostridium*, *Bifidobacterium*, and *Bacteroides*, but can promote the growth of insensitive enterococci, some lactobacilli and potentially pathogenic Enterobacteriaceae (Yin et al. 2015). Neomycin and penicillin can kill most gram-negative bacteria (Hazenberg et al. 1983). Metronidazole is used to treat microaerobic and anaerobic bacteria (Dingsdag and Hunter 2018) and increase the number of intestinal Lactobacilli (Ubeda and Pamer 2012). Amoxicillin can kill *Lactobacillus* and increase the number of drug-resistant Enterobacteriaceae (Jernberg et al. 2007). Therefore, the use of antibiotics not only destroys the dynamic balance of the host gut microbiota, but also has a large impact on the microbial metabolic environment of the whole intestinal tract and the microbial metabolic capacity of drugs. According to our findings, the liver damage in the ABx + TP group was more severe than that in the TP group. Similarly, Huang et al. found that the liver injury caused by the injection of TP (0.5 mg/kg) after the elimination of the gut microbiota using antibiotics was more serious than that in the TP group. However, the phenomenon of severe liver injury could be reversed after bacterial transplantation. Huang et al. proposed that this result is related to the protective effect of propionate derived from the intestinal microbiota on TP and the fact that TP restricts the growth of Firmicum, resulting in a lack of SCFAs in the cecum (Huang et al. 2020). In addition, Ma et al. showed that the imbalance of gut microbiota caused by antibiotics would lead to autoimmune hepatitis, and transplantation of fecal microbiota could significantly reduce gut microbiota-mediated liver injury in mice (Ma et al. 2021). Proton pump inhibitor (PPI) or long-term antibiotic (ABx) intake will cause an imbalance of the gut microbiota. Multivariate Cox regression analysis showed that the risk of acute liver failure (ALF) in the population taking PPI or ABx is significantly increased. Animal experiments showed that the gut microbiota diversity of male Nlrp6 $^{-/-}$ mice was reduced after the injection of sublethal doses of paracetamol (APAP) or lipopolysaccharide (LPS), which led to the production of ALF (Schneider et al. 2021). These studies prove that there is a close relationship between the gut microbiota and liver injury.

Colonization by exogenous microorganisms has been studied in many countries. A variety of human fecal species from the *Bacteroides* can successfully colonize the guts of antibiotic-treated and non-antibiotic-treated mice (Zhou et al. 2018). However, there are many challenges for the entry of exogenous microorganisms into the host, e.g., the gut environment (pH gradient, oxygen concentration) of the host (Evans et al. 1988;Albenberg et al. 2014), and rejection by the host immune system (Belkaid and Hand 2014). In addition, the host genotype and microbiota also affect the colonization capacity of foreign microorganisms (Dong et al. 2021). Moreover, the gut microbiota of mice that were not treated with antibiotics was resistant to colonization by human fecal species, resulting in the reduced abundance and taxonomic diversity of transplanted fecal species (Zhou et al. 2018). In previous microbiota colonization experiments, antibiotics are usually given first, and then microbiota colonization is performed (Li et al. 2019). Therefore, in this study, we first used four consecutive antibiotics to remove most of the gut microbiota of the mice and then used LGG and BF to colonize the mice for 4 weeks. Relevant studies have confirmed the protective effect of these two strains on liver injury (Pagliuca et al. 2016;Liu et al. 2020). Our results showed that the degree of liver injury in mice after colonization of the two strains was reduced according to the biochemical indicators, liver pathology, and liver appearance; however, it could not completely resist the liver injury caused by TP. It is speculated that a single gut microbiota cannot completely alleviate the liver injury caused by TP because of the complexity of the host gut microbiota, which is also a defect of the method of microbial colonization after antibiotic treatment. However, this study still showed that LGG and BF play an important role in liver injury caused by TP.

For a long time, researchers have focused on the toxicity of TP in the liver and kidney, with little focus on gastrointestinal toxicity. However, many studies have confirmed that the oral administration of TW preparations is likely to cause gastrointestinal adverse reactions, such as nausea, anorexia, vomiting, diarrhea, gastrointestinal ulcers, and bleeding (Wang et al. 2012;Zhou et al. 2012). Yuman et al. analyzed the adverse reactions to TW preparations in Henan Province from 2004 to 2019. Among the adverse reactions to TW preparations, gastrointestinal damage accounted for 54.68%, with nausea and vomiting as the main manifestations (Li et al. 2020). This reflects that TW and related preparations cause a certain amount of damage to the gastrointestinal tract. Therefore, our study paid attention to whether TP could cause intestinal injury. We found that TP could not cause obvious intestinal injury in normal mice by gavage, but administration of TP after administration of antibiotics caused a gut microbiota disorder, which resulted in severe damage to the ileum of mice. This suggests that the gut microbiota has an important influence on TPinduced intestinal injury, and TP-induced intestinal injury is closely related to the aggravation of liver injury after flora disorder.

Proteins represent the intermediate phenotype of disease and are also the focus of life science research. Their correlation with the gene expression levels provide valuable insights to reveal new drug targets and biomarkers, and to further explore drug and disease-related mechanisms (Suhre et al. 2021). Therefore, we used proteomics to further analyze the cause of TP-induced ileal injury. We identified 272 significantly differentially abundant proteins between the CON group and ABx + TP group. KEGG pathway analysis of these differentially abundant proteins indicated significant changes were in retinol metabolism, steroid hormone biosynthesis, linoleic acid metabolism, drug metabolism, cytochrome P450, chemical

carcinogen DNA adduct, and other important pathways. Among the pathways, the retinol metabolic pathway changed significantly, and 11 differentially abundant proteins were enriched in this pathway, namely retinal dehydrogenase 1, UDP-glucuronosyltransferase 1–1, aldehyde dehydrogenase, cytosolic 1, cytochrome P450 3A13, diacylglycerol O-acyltransferase 1, retinol dehydrogenase 7, 17-beta-hydroxysteroid dehydrogenase type 6, UDP-glucuronosyltransferase 2A3, cytochrome P450 2C40, all-trans-retinol 13,14-reductase, and Cytochrome P450 2C70. Retinol metabolism plays an important role in liver diseases and retinol can activate hepatic stellate cells (HSC) to become myofibroblasts (MFBs) to induce liver injury (Saeed et al. 2017). NAFLD is also related to the level of retinol in the serum and liver. NAFLD can cause cell-specific rearrangement in retinol metabolism, leading to the accumulation of retinol in liver cells. Retinol metabolism is closely related to the intestinal mucosal barrier and intestinal immunity. Therefore, retinol metabolism plays an important role in the balance of the intestinal mucosal barrier and liver diseases, suggesting that it is a key target to connect the gut-liver axis.

The KEGG analysis results showed that linoleic acid metabolism also changed significantly. It has been reported that retinol metabolism is closely related to linoleic acid metabolism. Conjugated linoleic acid (CLA) can regulate retinol metabolism, and can activate peroxisomes, increase free retinol levels, and affect related gene expression by activating the peroxisome proliferator-activated receptor (Carta et al. 2014). It has also been suggested that linoleic acid metabolism might play an important role in intestinal and liver injury induced by TP. Cytochrome P450 proteins play an important role in drug metabolism, especially in the liver. A genetic polymorphism of the CYP450 enzyme may be an important reason for individual differences in drug-induced liver injury (Wang and Zou 2020). Many studies have confirmed that TP can affect the activity of CYP450 enzymes. TP can cause hepatotoxicity by reducing the transcriptional activity and protein expression of CYP450 subtypes CYP3A, CYP2C9, CYP2C19, and CYP2E1. In addition, mRNA levels in four major subtypes of the CYP3A family (3A1/3A23, 3A2, 3A9, and 3A62), CYP2C9, CYP2C19, and CYP2E1 decreased in a dose-dependent manner after TP treatment (Lu et al. 2017). However, some studies have shown that gut microbiota can also affect the activity of the CYP450 enzyme. For example, the mRNA and protein expression level of CYP3A were higher than those of sterile mice after the mice were given antibiotics in the SPF environment, indicating that changes in gut microbiota can change the expression and activity of drug-metabolizing enzymes in the liver (Ishii et al. 2012). This suggests that both gut antibiotic-induced microbiota disorders and TP can affect CYP450 enzyme activity and thus affect the toxicity of TP to the liver and intestine. Our results also confirmed the effect of TP on CYP450 enzymes. The results of the proteomic analysis showed that the levels of CYP2D11, CYP2D26, CYP2C70, CYP4V2, CYP2C40, CYP2J6, CYP3A13, CYP27A1, CYP4B1, CYP4F14, CYP3A25, and CYP2E1 were different among groups, indicating that TP could also affect the activity of intestinal CYP450 enzymes. Previous research showed that the activity of CYP450 enzyme in intestine is in the order CYP3A4 > CYP2C9 > CYP2C19 > CYP2J2 > CYP4F2. Among them, CYP3A4, CYP2C9, CYP2C19, and CYP2J2 have the highest mRNA expression levels (> 5%) in all intestinal segments (Clermont et al. 2019). Research also suggests that CYP450 enzymes are related to intestinal toxicity. For example, diclofenac sodium can induce intestinal ulcers in humans and mice. The number of mice with intestinal ulcers induced by diclofenac sodium decreased after the gene encoding a specific CYP450 enzyme was

knocked out, which strongly supports the important role of CYP450 enzymes in the intestinal toxicity induced by diclofenac sodium (Zhu and Zhang 2012).

A DNA adduct is a substance with a carcinogenic effect and is one of the most important factors at the initial stage of the carcinogenic process. Moreover, covalent binding of DNA adducts is the cause of tumor occurrence and is now evaluated as an important indicator for the diagnosis of chemical carcinogenesis. Significant differences in 10 specific DNA adducts were observed in the small intestine tissues of GF mice and conventionally reared mice (Hsiao et al. 2020). This indicated that the gut microbiota had an important influence on the formation of DNA adducts. Steroids are related to enteritis, and steroids are considered as the main method to treat severe ulcerative colitis (Parida and Sharma 2019). The peroxisome pathway is among several pathways enriched for differentially abundant proteins. Research has shown that peroxisomes can mediate an epithelial repair mechanism and relieve colitis symptoms in mice (Du et al. 2020).

The above metabolic pathways provide a theoretical basis for the study of the mechanism of TP-induced intestinal injury. We also focused on intestinal barrierrelated proteins. The results showed that the proteins associated with the physical or chemical barrier related to intestinal injury did not change significantly, while the levels of two intestinal immune barrier proteins, REG3B and REG3G, were significantly reduced in the ABx + TP group. We speculated that REG3B and REG3G play an important role in the intestinal and liver injury caused by TP mediated by a disordered gut microbiota. The intestinal tract relies on various physical and biochemical barriers, such as IgA, the mucus layer, tight junctions, and antimicrobial peptides (AMPs) to prevent pathogens from entering the host. It plays an irreplaceable role in maintaining the balance between the internal and external environment and the immune system, helping the human body digest and absorb nutrients, and maintaining the health of the host (Kelsen et al. 2015). When the integrity of the intestinal barrier is lost, it will activate immune cells and lead to chronic inflammation of intestinal tissue. Inflammatory molecules can reach different organs through circulation and play a role in the pathogenesis of non-intestinal diseases, such as alcoholic and non-alcoholic liver diseases, diabetes, obesity, and chronic kidney disease (Yuan et al. 2019). AMPs are part of the innate immune response from prokaryotes to humans (Mahlapuu et al. 2016). A variety of AMPs, including defensins, lysozyme, and C-type lectin, are produced by epithelial cells and circulating immune cells of tissues, including the skin, respiratory tract, and intestinal tract (Müller et al. 2005;Salzman et al. 2009;Gallo and Hooper 2012), which help the host defend against microorganisms through various innate immune responses (Mukherjee et al. 2008; Lai and Gallo 2009). Among these AMPs, REG3 lectin is largely expressed in intestinal cells and Paneth cells of the small intestine and exerts a bactericidal activity as part of a host defense mechanism in the gut (Ogawa et al. 2003). The antimicrobial peptides REG3B and REG3G belong to the C-type lectins (Vaishnava et al. 2011) and are mainly expressed in the gastrointestinal tract under steady-state conditions. REG3B kills gram-negative bacteria and protects the mouse gut from infection (Miki et al. 2012). The proteomic results showed that REG3B and REG3G were significantly downregulated in the ileum tissue of the ABx + TP group, suggesting that TP-induced intestinal injury after gut microbiota disturbance is related to the impaired immune barrier and activation of the immune system. Meanwhile, the liver is the central organ of the immune system and contains a

variety of immune cells, including Kupffer cells, natural killer cells, dendritic cells, and hepatic sinusoidal endothelial cells (Thomson and Knolle 2010). It has been reported that liver injury caused by TP is associated with the immune system, and that TP play an important role in the development and functional differentiation of Th17/Treg subsets through NF-κB and p53 (Ruan and Chen 2012;Wang et al. 2014). This suggests that REG3B and REG3G can mediate immune responses leading to disruption of the gut immune barrier, which might play an important role in gut microbiota-mediated TP through the gut-liver axis to induce liver injury.

Conclusion

In the present study, we explored the effect and mechanism of TP-induced liver injury from the perspective of the gut-liver axis. We first discovered that gut microbiota disturbances can mediate TP-induced intestinal damage and aggravate liver damage in mice. *Lactobacillus* and *Bacteroides* are closely related to TP hepatotoxicity, colonization by which can alleviate liver and intestinal injury. Meanwhile, we also demonstrated that TP could elicit the liver immune response, and the disturbance of the gut microbiota can amplify the liver immune response, causing significant changes in the gut immune barrier proteins REG3B and REF3G and triggering changes to metabolite levels, such as the taurocholic acid, asparagine, leucine, and butyric acid. Collectively, the gut microbiota plays an important role in exaggerating TP–induced liver injury via the gut–liver axis.

Declarations

Ethical Approval

The relevant animal experiments were reviewed and approved by the experimental animal ethics committee of Shanghai University of traditional Chinese medicine (PZSHUTCM210507014), and the relevant experimental operations were carried out in accordance with the regulations on the protection of experimental animals.

Competing Interests

The authors have no relevant financial or non-financial interests to disclose.

Author Contributions

WY, HY and YT conceived the study. WY performed the experiments and wrote the manuscript. HY and LY participated in the experiment and data processing. ZH participated in the animal treatment. ZH and CL provided resources and funding acquisition. YT reviewed and edited the manuscripts and contributed to funding acquisition. All authors read and approved the final version of manuscript.

Funding

This work was supported by grants from the Science and Technology Support Project of Shanghai Science and Technology Commission [grant numbers 18401900700, 20S21901800] and the Three-Year Action Plan for Development of TCM in Shanghai [grant number ZY3-CCCX-2-1003].

Availability of data and materials

All data in this study are available from the corresponding author upon reasonable request.

References

1. Albenberg L, Esipova TV, Judge CP, et al. Correlation Between Intraluminal Oxygen Gradient and Radial Partitioning of Intestinal Microbiota in Humans and Mice. Gastroenterology. 2014;147(5): 1055-1063. https://doi.org/ 10.1053/j.gastro.2014.07.020.
2. Saeed A, Dullaart RPF, Schreuder TCMA,Blokzijl H, and Faber KN. Disturbed Vitamin A Metabolism in Non-Alcoholic Fatty Liver Disease (NAFLD). Nutrients. 2017;10(1):29. https://doi.org/ 10.3390/nu10010029.
3. Arvidsson C, Hallén A, and Bäckhed F. Generating and Analyzing Germ-Free Mice. Current protocols in mouse biology. 2012;2(4):307–316. https://doi.org/ 10.1002/9780470942390.mo120064.
4. Belkaid Y, and Hand TW. Role of the microbiota in immunity and inflammation. Cell. 2014;157(1):121-141. https://doi.org/10.1016/J.cell.
5. Caporaso JG, Kuczynski J, Stombaugh J, et al. QIIME allows analysis of high-throughput community sequencing data. Nature methods. 2020;7:335-336. https://doi.org/ 10.1038/nmeth.f.303.
6. Ubeda C, and Pamer EG. Antibiotics, microbiota, and immune defense. Trends in Immunology. 2012;33(9):459-466. https://doi.org/ 10.1016/j.it
7. Carmody RN, and Turnbaugh PJ. Host-microbial interactions in the metabolism of therapeutic and diet-derived xenobiotics. Journal of Clinical Investigation. 2014;124(10):4173-4181. https://doi.org/ 10.1172/JCI72335.
8. Carta G, Murru E, Cordeddu L, et al. Metabolic interactions between vitamin A and conjugated linoleic acid. Nutrients. 2014;6(3):1262–1272. https://doi.org/ 10.3390/nu6031262.
9. Chen X, Zhang YP, Xu J, and Liu Y. Modern research progress of triptolide. Journal of Guizhou University of Traditional Chinese Medicine. 2021;43(5):85-89. https://doi.org/ 10.16588/j.cnki.issn2096-8426.
10. Clarke G, Sandhu KV, Griffin BT, et al. Gut Reactions: Breaking Down Xenobiotic–Microbiome Interactions. Pharmacological Reviews. 2019;71(2):198-224. https://doi.org/ 10.1124/pr.118.015768.
11. Clermont V, Grangeon A, Barama A, et al. Activity and mRNA expression levels of selected cytochromes P450 in various sections of the human small intestine. British journal of clinical pharmacology. 2019;85(6):1367–1377. https://doi.org/ 10.1111/bcp.13908.

12. Cui YZ, Wang QJ, Chang RX, Zhou XC, and Xu C. Intestinal Barrier Function-Non-alcoholic Fatty Liver Disease Interactions and Possible Role of Gut Microbiota. Journal of Agricultural & Food Chemistry. 2019;67(10):2754-2762. https://doi.org/ 10.1021/acs.jafc.9b00080.
13. Desantis TZ, Hugenholtz P, Larsen N, Rojas M, and Andersen GL. Greengenes, a Chimera-Checked 16S rRNA Gene Database and Workbench Compatible with ARB. Applied & Environmental Microbiology. 2006;72(7):5069-5072. https://doi.org/ 10.1128/AEM.03006-05.
14. Ding L, Gong YH, Yang ZF, et al. Lactobacillus rhamnosus GG Ameliorates Liver Injury and Hypoxic Hepatitis in Rat Model of CLP-Induced Sepsis. Digestive Diseases and Sciences. 2019;64(10): 2867-2877. https://doi.org/ 10.1007/s10620-019-05628-0.
15. Dingsdag SA, and Hunter N. Metronidazole: an update on metabolism, structure-cytotoxicity and resistance mechanisms. The Journal of antimicrobial chemotherapy. 2018;73(2):265–279. https://doi.org/ 10.1093/jac/dkx351.
16. Du G, Xiong L, Li X, et al. Peroxisome Elevation Induces Stem Cell Differentiation and Intestinal Epithelial Repair. Developmental cell. 2020;53(2):169–184. https://doi.org/ 10.1016/j.devcel.2020.03.002.
17. Edgar R. UPARSE: highly accurate OTU sequences from microbial amplicon reads. Nat Methods 2013;10:996–998. https://doi.org/10.1038/nmeth.2604.
18. Evans DF, Pye G, Bramley R, et al. Measurement of gastrointestinal pH profiles in normal ambulant human subjects. Gut. 1998;29(8):1035-1041. https://doi.org/10.1136/gut.29.8.1035.
19. Fan D, Guo Q, Shen J, et al. The Effect of Triptolide in Rheumatoid Arthritis: From Basic Research towards Clinical Translation. International journal of Molecular Sciences. 2018;19(2):376. https://doi.org/ 10.3390/ijms19020376.
20. Feng W, Ao H, and Peng C. Gut Microbiota, Short-Chain Fatty Acids, and Herbal Medicines. Frontiers in Pharmacology. 2018;9:1354. https://doi.org/10.3389/fphar.2018.01354.
21. Filliol A, Piquet-Pellorce C, Raguénès-Nicol C, et al. RIPK1 protects hepatocytes from Kupffer cells-mediated TNF-induced apoptosis in mouse models of PAMP-induced hepatitis. Journal of Hepatology. 2017;66(6):1205. https://doi.org/10.1016/j.jhep.2017.01.005.
22. Angelucci F, Cechova K, Amlerova J, and Hort J. Antibiotics, gut microbiota, and Alzheimer's disease. J Neuroinflammation. 2019;16(1):108. https://doi.org/10.1186/s12974-019-1494-4.
23. Gallo RL, and Hooper LV. Epithelial antimicrobial defence of the skin and intestine. Nature Reviews Immunology. 2012;12(7):503-516. https://doi.org/10.1038/nri3228.
24. Henao-Mejia1 J, Elinav E, Jin CC, et al. Inflammasome-mediated dysbiosis regulates progression of NAFLD and obesity. Nature. 2012;482(7384): 179-185. https://doi.org/10.1038/nature10809.
25. Hou Z, Chen L, Fang P, et al. Mechanisms of Triptolide-Induced Hepatotoxicity and Protective Effect of Combined Use of Isoliquiritigenin: Possible Roles of Nrf2 and Hepatic Transporters. Front. Pharmacol. 2018;9:226. https://doi.org/10.3389/fphar.2018.00226.
26. Hsiao YC, Liu CW, Chi L, Yang Y, and Lu K. Effects of Gut Microbiome on Carcinogenic DNA Damage. Chemical research in toxicology. 2020;33(8):2130–2138. https://doi.org/

10.1021/acs.chemrestox.0c00142.

27. Huang JF, Zhao Q, Dai MY, et al. Gut microbiota protects from triptolide-induced hepatotoxicity: Key role of propionate and its downstream signalling events. Pharmacological research. 2020;155: 104752. https://doi.org/10.1016/j.phrs.2020.104752.
28. Ishii M, Toda T, Ikarashi N, Ochiai W, and Sugiyama K. Effects of intestinal flora on the expression of cytochrome P450 3A in the liver. Journal of the Pharmaceutical Society of Japan. 2012;132(3): 301–310. https://doi.org/10.1248/yakushi.132.301.
29. Jernberg C, Löfmark S, Edlund C, and Jansson JK. Long-term ecological impacts of antibiotic administration on the human intestinal microbiota. ISME Journal. 2007;7(1):56-66. https://doi.org/10.1038/ismej.2007.3.
30. Ho JTK, Chan GCF, and Li JCB. Systemic effects of gut microbiota and its relationship with disease and modulation. Bmc Immunology. 2015;16(1):1-6. https://doi.org/10.1186/s12865-015-0083-2.
31. Kalantar-Zadeh K, Berean KJ, and Burgell RE. Intestinal gases: influence on gut disorders and the role of dietary manipulations. Nature Reviews Gastroenterology & Hepatology. 2019;16:733–747. https://doi.org/10.1038/s41575-019-0193-z.
32. Kelsen JR, Baldassano RN, Artis D, and Sonnenberg GF. Maintaining Intestinal Health: The Genetics and Immunology of Very Early Onset Inflammatory Bowel Disease. Cellular and Molecular Gastroenterology and Hepatology. 2015;1(5):462-476. https://doi.org/ 10.1016/j.jcmgh.2015.06.010.
33. Kim CH, Park J and Kim M. Gut microbiota-erived short-chain fatty acids, T cells, and inflammation. Immune Network. 2014;14(6):277–288. https://doi.org/10.4110/in.2014.14.6.277.
34. Koppel N, Rekdal VM, and Balskus EP. Chemical transformation of xenobiotics by the human gut microbiota. Science. 2017;356(6344):1246-1257. https://doi.org/10.1126/science.aag2770.
35. Kupchan SM, Court WA, Dailey RG, Gilmore CJ, and Bryan RF. Triptolide and tripdiolide, novel antileukemic diterpenoid triepoxides from Tripterygium wilfordii. Journal of the American Chemical Society. 1972;94(20):7194-7195. https://doi.org/ 10.1021/ja00775a078.
36. Lam KN, Alexander M, and Turnbaugh PJ. Precision Medicine Goes Microscopic: Engineering the Microbiome to Improve Drug Outcomes. Cell Host Microbe. 2019;26(1):22-34. https://doi.org/10.1016/j.chom.2019.06.011.
37. Li G, Ren J, Wang G , et al. T2 enhances in situ level of Foxp3+ regulatory cells and modulates inflammatory cytokines in Crohn's disease. International Immunopharmacology. 2014;18(2): 244-248. https://doi.org/10.1016/j.intimp.2013.12.014.
38. Li N, Wang Q, Wang Y, et al. Fecal microbiota transplantation from chronic unpredictable mild stress mice donors affects anxiety-like and depression-like behavior in recipient mice via the gut microbiota-inflammation-brain axis. Stress. 2019;22(5):592-602. https://doi.org/10.1080/10253890.2019.1617267.
39. Li YM, Chen, SW, Xia, XD, et al. Analysis on adverse reactions caused by preparations containing Tripterygium wilfordii in Henan Province from 2004 to 2019. Drugs & Clinic. 2020;35(5):988-994. https://doi.org/10.7501/j.issn.1674-5515.2020.05.036.

40. Liu M, Yuan J, Hu WJ, and Ke CQ. Pretreatment with broad-spectrum antibiotics alters the pharmacokinetics of major constituents of Shaoyao-Gancao decoction in rats after oral administration. Acta Pharmacologica Sinica. 2019;40(2):288-296. https://doi.org/ 10.1038/s41401-018-0011-0.
41. Liu YT, Hu YQ, Wang YL, et al. Antibiotic pretreatment promotes orally-administered triptolide absorption and aggravates hepatotoxicity and intestinal injury in mice. Journal of Ethnopharmacology. 2022;292:115224. https://doi.org/10.1016/j.jep.2022.115224.
42. Lu Y, Xie T, Zhang Y, et al. Triptolide Induces hepatotoxicity via inhibition of CYP450s in Rat liver microsomes. BMC complementary and alternative medicine. 2017;17(1):1-15. https://doi.org/ 10.1186/s12906-016-1504-3.
43. Hazenberg MP, Boom MVD, Bakker M, et al. Effect of antibiotics on the human intestinal flora in mice. Antonie van Leeuwenhoek. 1983;49(2):97–109. https://doi.org/10.1007/BF00393667.
44. Ma L, Zhang LW, Song JG, et al. Fecal Microbiota Transplantation Controls Progression of Experimental Autoimmune Hepatitis in Mice by Modulating the TFR/TFH Immune Imbalance and Intestinal Microbiota Composition. Frontiers in immunology. 2019;8(6):728723. https://doi.org/ 10.3389/fimmu.2021.728723.
45. Mahlapuu M, Håkansson J, Ringstad L, and Björn C. Antimicrobial Peptides: An Emerging Category of Therapeutic Agents. Frontiers in cellular and infection microbiology. 2016;6:194. https://doi.org/10.3389/fcimb.2016.00194.
46. Mantegazza C, Molinari P, D'auria E, Sonnino M, Morelli L, and Zuccotti GV. Probiotics and antibiotic-associated diarrhea in children: A review and new evidence on Lactobacillus rhamnosus GG during and after antibiotic treatment. Pharmacological research. 2018;128:63-72. https://doi.org/10.1016/j.phrs.2017.08.001.
47. Miki T, Holst O, and Hardt WD. The Bactericidal Activity of the C-type Lectin RegIIIβ against Gram-negative Bacteria involves Binding to Lipid A. Journal of Biological Chemistry. 2012;287(41): 34844-34855. https://doi.org/10.1074/jbc.M112.399998.
48. Mukherjee S, Vaishnava S, and Hooper LV. Multi-layered regulation of intestinal antimicrobial defense. Cellular & Molecular Life Sciences. 2008;65(19):3019-3027. https://doi.org/ 10.1007/s00018-008-8182-3.
49. Müller C, Autenrieth IB, and Peschel A. Innate defenses of the intestinal epithelial barrier. Cellular & Molecular Life Sciences. 2005;62(12):1297. https://doi.org/10.1007/s00018-005-5034-2.
50. Nakamoto N, Amiya T, Aoki R, Taniki N, Koda Y, and Miyamoto K. Commensal lactobacillus controls immune tolerance during acute liver injury in mice. Cell Reports. 2017;21(5):1215-1226. https://doi.org/10.1016/j.celrep.2017.10.022.
51. Ni L, and Zhang B. Study on toxicity theory of Chinese materia medica based on organism state. China Journal of Traditional Chinese Medicine and Pharmacy. 2009;24(5):549-551. https://doi.org/ CNKI:SUN:BXYY.0.2009-05-002.

52. Nicholson JK, Holmes E, Kinross J, Burcelin R, Gibson G, Jia W, et al. Host-Gut Microbiota Metabolic Interactions. Science. 2012;336(6086):1262-1267. https://doi.org/10.1126/science.1223813.
53. Ogawa H, Fukushima K, Naito H, et al. Increased expression of HIP/PAP and regenerating gene III in human inflammatory bowel disease and a murine bacterial reconstitution model. Inflammatory Bowel Diseases. 2003;9(3):162-170. https://doi.org/10.1097/00054725-200305000-00003.
54. Pagliuca C, Cicatiello AG, Colicchio R, et al. Novel Approach for Evaluation of Bacteroides fragilis Protective Role against Bartonella henselae Liver Damage in Immunocompromised Murine Model. Frontiers in microbiology. 2016;7:1750. https://doi.org/10.3389/fmicb.2016.01750.
55. Parida S, and Sharma D. The Microbiome-Estrogen Connection and Breast Cancer Risk. Cells. 2019;8(12):1642. https://doi.org/10.3390/cells8121642.
56. Pleasants JR. Rearing germ-free cesarean-born rats, mice and rabbits through weaning. Annals of the New York Academy of Sciences. 1959;78:116-126. https://doi.org/10.1111/j.1749-6632.1959.tb53099.x.
57. Ren L, Song Q, Liu Y, Zhang L, and Feng W. Probiotic lactobacillus rhamnosus gg prevents progesterone metabolite epiallaopregnanolone sulfate-induced hepatic bile acid accumulation and liver injury. Biochemical and Biophysical Research Communications. 2019;520(1):1-6. https://doi.org/ 10.1016/j.bbrc.2019.09.103.
58. Ruan Q, and Chen YH. Nuclear factor-κB in immunity and inflammation: the Treg and Th17 connection. Springer New York. 2012;946:207-221. https://doi.org/10.1007/978-1-4614-0106-3_12.
59. Dong SS, Zeng BH, Hu L, et al. Effect of a Humanized Diet Profile on Colonization Efficiency and Gut Microbial Diversity in Human Flora-Associated Mice. Frontiers in Nutrition. 2021;8:633738. https://doi.org/10.3389/fnut.2021.633738.
60. Salzman NH, Hung K, Haribhai D, Chu H, and Bos NA. Enteric defensins are essential regulators of intestinal microbial ecology. Nature Immunology. 2009;11(1):76-83. https://doi.org/ 10.1038/ni.1825.
61. Schneider KM, Elfers C, Ghallab A, Schneider CV, Galvez E, Mohs A, et al. Intestinal Dysbiosis Amplifies Acetaminophen-Induced Acute Liver Injury. Cellular and molecular gastroenterology and hepatology. 2021;11(4):909–933. https://doi.org/10.1016/j.jcmgh.2020.11.002.
62. Seki E, and Schnabl B. Role of innate immunity and the microbiota in liver fibrosis: crosstalk between the liver and gut. Journal of Physiology. 2012;590(3):447-458. https://doi.org/ 10.1113/jphysiol.2011.219691.
63. Suhre K, Mccarthy MI, and Schwenk JM. Genetics meets proteomics: perspectives for large population-based studies. Nature reviews. Genetics. 2021;22(1):19–37. https://doi.org/10.1038/s41576-020-0268-2.
64. Thomson AW, and Knolle PA. Antigen-presenting cell function in the tolerogenic liver environment. Nature Reviews Immunology. 2010;10(11):753. https://doi.org/10.1038/nri2858.
65. Tilg H, Cani PD, and Mayer EA. Gut microbiome and liver diseases. Gut. 2016;65(12):2035–2044. https://doi.org/10.1136/gutjnl-2016-312729.

66. Tulstrup MVL, Christensen EG, Carvalho V, et al. Antibiotic Treatment Affects Intestinal Permeability and Gut Microbial Composition in Wistar Rats Dependent on Antibiotic Class. PLoS ONE. 2015;10(12):e0144854. https://doi.org/10.1371/journal.pone.0144854.
67. Uribe-Herranz M, Rafail S, Beghi S, et al. Gut microbiota modulate dendritic cell antigen presentation and radiotherapy-induced antitumor immune response. The Journal of clinical investigation. 2020;130(1):466–479. https://doi.org/10.1172/JCI124332.
68. Vaishnava S, Yamamoto M, Severson KM, Ruhn KA, and Hooper LV. The Antibacterial Lectin RegIIIgamma Promotes the Spatial Segregation of Microbiota and Host in the Intestine. Science. 2011;334(6053):255-258. https://doi.org/10.1126/science.1209791.
69. Wallace BD, Roberts AB, Pollet RM, et al. Structure and Inhibition of Microbiome β-Glucuronidases Essential to the Alleviation of Cancer Drug Toxicity. Chemical Biology. 2015;22(9):1238-1249. https://doi.org/10.1016/j.chembiol.2015.08.005.
70. Wan J, Benkdane M, Teixeira-Clerc F, et al. M2 Kupffer cells promote M1 Kupffer cell apoptosis: a protective mechanism against alcoholic and nonalcoholic fatty liver disease. Hepatology. 2014;59(1):130-142. https://doi.org/10.1002/hep.26607.
71. Wang B, Jiang Z, and Zhang L. Advances in studies on toxicity and attenuation of triptolide. Drug Evaluation Research. 2012;35:211–215. https://doi.org/ 10.7501/j.issn.0253-6376.
72. Wang J, Chu Y, and Zhou X. Inhibitory effect of Triperygium wilfordii polyglucoside on dipeptidyl peptidase I in vivo and in vitro. Biomedicine & pharmacotherapy. 2017;96:466-470. https://doi.org/10.1016/j.biopha.2017.09.139.
73. Wang MH, Wang X, Yan YJ, Huang ZY, Wang Q, and Wen HR. Correlation Between Triptolide in Tripterygium Glycoside Tablets and Hepatotoxicity in vitro. Modern Chinese Medicine. 2021;8: 1344-1351. https://doi.org/ 10.13313/j.issn.1673-4890.20200520001.
74. Wang QH, and Hu M. Pharmacological and Toxic Effects of Tripterygium wilfordii. China Pharmaceuticals. 2010;19(17):85-86. https://doi.org/10.3969/j.issn.1006-4931.2010.19.061.
75. Wang QL, and Zou ZS. Association between cytochrome P450 gene polymorphism and drug-induced liver injury. Journal of Clinical Hepatology. 2020;36(5):1150-1153. https://doi.org/ 10.3969/j.issn.1001-5256.2020.05.045.
76. Wang XZ, Jiang ZZ, Cao WP, Yuan ZQ, Sun LX, and Zhang LY. Th17/Treg imbalance in triptolide-induced liver injury. Fitoterapia. 2014;93:245-251. https://doi.org/10.1016/j.fitote.2014.01.006.
77. Wang YH, Liu YL, Kirpich I, et al. Lactobacillus rhamnosus GG reduces hepatic TNF alpha production and inflammation in chronic alcohol-induced liver injury. Journal of Nutritional Biochemistry. 2013;24(9):1609-1615. https://doi.org/10.1016/j.jnutbio.2013.02.001.
78. Zhou W, Chow KH, Fleming E, and Oh J. Selective colonization ability of human fecal microbes in different mouse gut environments. The ISME Journal. 2018;13(3):805-823. https://doi.org/ 10.1038/s41396-018-0312-9.
79. Wiśniewski JR, Zougman A, Nagaraj N, and Mann M. Universal sample preparation method for proteome analysis. Nature Methods. 2009;6(5):359-362. https://doi.org/10.1038/nmeth.1322.

80. Wostmann BS, Larkin C, Moriarty A, and Bruckner-Kardoss E. Dietary intake,energy metabolism, and excretory losses of adult male germfree Wistar rats. Laboratory animal science. 1983;33(1): 46–50. https://doi.org/ 10.2307/3808211.
81. Wu H, Rao Q, and Ma GC, et al. Effect of Triptolide on Dextran Sodium Sulfate-Induced Ulcerative Colitis and Gut Microbiota in Mice. Frontiers in Pharmacology. 2020;10:1652. https://doi.org/ 10.3389/fphar.2019.01652.
82. Zhou YY, Xuan X, Peng WK, et al. The Effectiveness and Safety of Tripterygium wilfordii Hook. F Extracts in Rheumatoid Arthritis: A Systematic Review and Meta-Analysis. Frontiers in Pharmacology. 2018;16(9):356. https://doi.org/10.3389/fphar.2018.00356.
83. Yang X, Lam CW, Xu H, et al. Preparation and Optimization of Triptolide-Loaded Solid Lipid Nanoparticles for Oral Delivery with Reduced Gastric Irritation. Molecules. 2013;18(11): 13340-13356. https://doi.org/10.3390/molecules181113340.
84. Yin J, Prabhakar M, Wang S, and Liao SX. Different Dynamic Patterns of β-Lactams, Quinolones, Glycopeptides and Macrolides on Mouse Gut Microbial Diversity. PLoS One. 2015;10(5): e0126712. https://doi.org/10.1371/journal.pone.0126712.
85. Lai Y, and Gallo RL. AMPed up immunity: how antimicrobial peptides have multiple roles in immune defense. Trends in Immunology. 2009;30(3):131-141. https://doi.org/10.1016/j.it.2008.12.003.
86. Yuan Z, Zhang H, Hasnat M, et al. A new perspective of triptolide-associated hepatotoxicity: Liver hypersensitivity upon LPS stimulation. Toxicology. 2019;414:45–56. https://doi.org/ 10.1016/j.tox.2019.01.005.
87. Liu YH, Chen KF, Li FY, et al. Probiotic Lactobacillus rhamnosus GG prevents liver fibrosis through inhibiting hepatic bile acid synthesis and enhancing bile acid excretion in mice. Hepatology. 2020;71:2050-2066. https://doi.org/10.1002/hep.30975.
88. Zhou ZL, Yang YX, Ding J, Li YC, and Miao ZH. Triptolide: Structural modifications, structure-activity relationships, bioactivities, clinical development and mechanisms. Natural Product Reports. 2012;29(4):457–475. https://doi.org/10.1039/c2np00088a.
89. Zhu Y, and Zhang QY. Role of intestinal cytochrome p450 enzymes in diclofenac-induced toxicity in the small intestine. The Journal of pharmacology and experimental therapeutics. 2012;343(2):362–370. https://doi.org/10.1124/jpet.112.198077.
90. Zhua SQ, Liu J, Han B, et al. Fluoride exposure cause colon microbiota dysbiosis by destroyed microenvironment and disturbed antimicrobial peptides expression in colon. Environmental Pollution. 2021;292:118381. https://doi.org/10.1016/j.envpol.2021.118381.
91. Zhuge A, Li B, Yuan Y, Lv L, and Li L. Lactobacillus salivarius li01 encapsulated in alginate-pectin microgels ameliorates d-galactosamine-induced acute liver injury in rats. Applied Microbiology and Biotechnology. 2020;104(3):7437–7455. https://doi.org/10.1007/s00253-020-10749-y.
92. Zimmermann M, Zimmermann-Kogadeeva M, Wegmann R, and Goodman AL. Mapping human microbiome drug metabolism by gut bacteria and their genes. Nature 2019;570(7762):462–467. https://doi.org/10.1038/s41586-019-1291-3.

93. Zorn AM, and Wells JM. Vertebrate Endoderm Development and Organ Formation. Annual Review of Cell & Developmental Biology. 2009;25(1):221-251. https://doi.org/10.1146/annurev.cellbio.042308.113344.

Figures

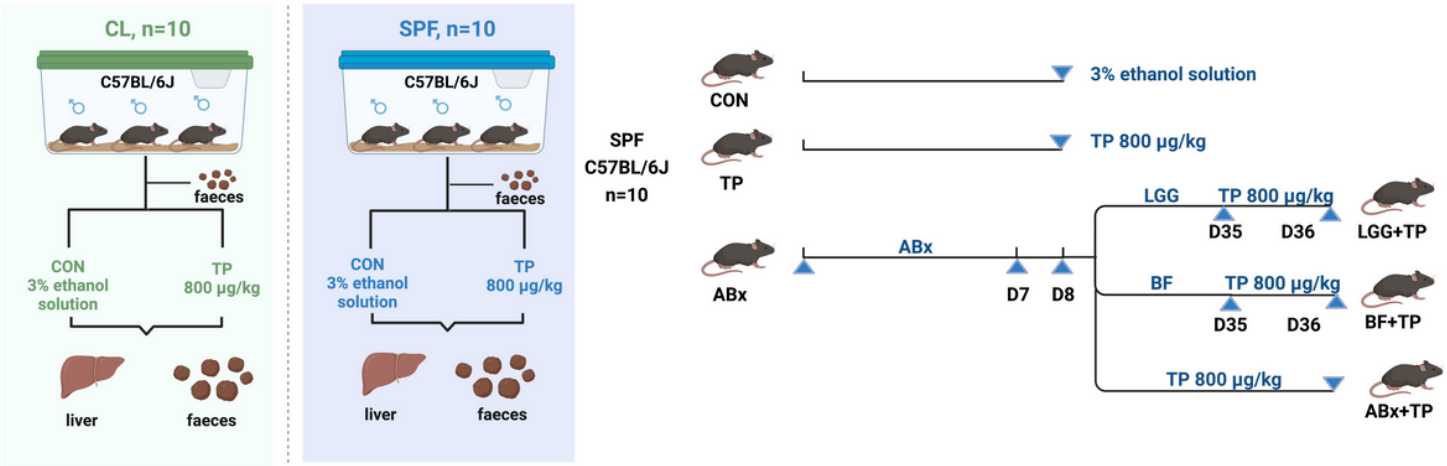


Figure 1

Schematic Diagram of Animal Grouping.

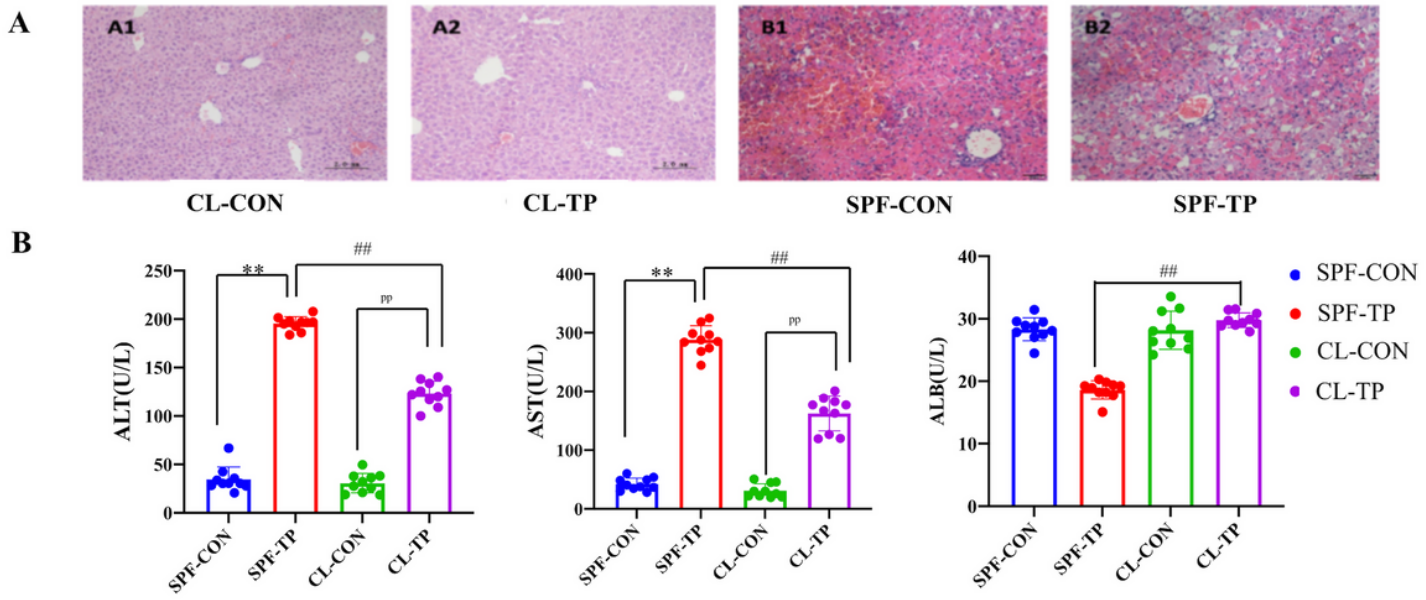


Figure 2

(A) H&E staining of liver tissue. (B) AST, ALT, and ALB levels in serum.

Note: SPF-CON: 3% ethanol solution was administered under the SPF environment (n = 10); SPF-TP: 800 μg/kg TP solution was administered under the SPF environment (n = 10); CL-CON: 3% ethanol solution was administered in the clean environment (n = 10); CL-TP: 800 μg/kg TP solution was administered in the clean environment (n = 10)

Data are shown as the mean ± SD. Compared with SPF-CON group, $^{**}P < 0.01$; Compared with CL-CON group, $^{\#\#}P < 0.01$; Compared with SPF-TP group, $^{▲▲}P < 0.01$.

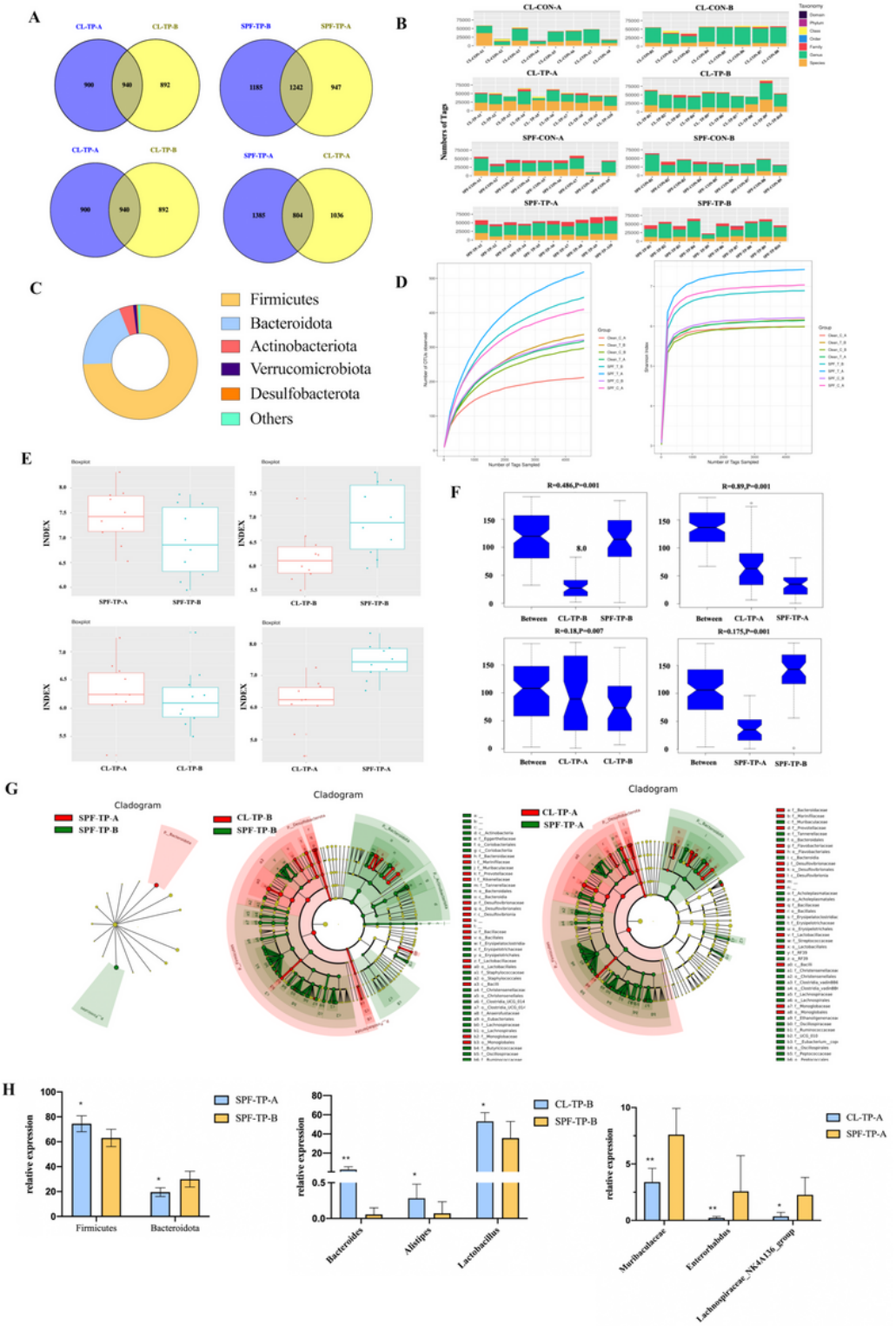


Figure 3

(A) Venn diagram of the OTU comparison between different groups. (B) Stacked histogram of sample expression at each classification level. (C) The main and the secondary phyla of the samples. (D) Species dilution curve and Shannon curve of the test groups (The abscissa is the number of tags, and the ordinate is the Shannon value obtained when extracting the corresponding number of tags). (E) Shannon index Boxplot of each comparison group. (F) Unweighted ANOISM analysis of the groups. (G)

Evolutionary branch diagram of differential microbial analysis in mice (Each small circle represents a classification under the corresponding level, and the diameter of the circle corresponds to the relative abundance). (H) Major differential genera between the groups.

Note: SPF-TP-B: before administration of TP solution in the SPF environment (n = 10); SPF-TP-A: After administration of TP solution 800 μg/kg in the SPF environment (n = 10); SPF-CON-B: before administration of 3% ethanol solution in the SPF environment (n = 9); SPF-CON-A: after administration of 3% ethanol solution in the SPF environment (n = 9); CL-CON-B: before administration of 3% ethanol solution in the clean environment (n = 8); CL-CON-A: after administration of 3% ethanol solution in the clean environment (n = 8); CL-TP-B: before administration of TP solution in the clean environment (n = 10); CL-TP-A: after administration of TP solution 800 μg/kg in the clean environment (n = 10).

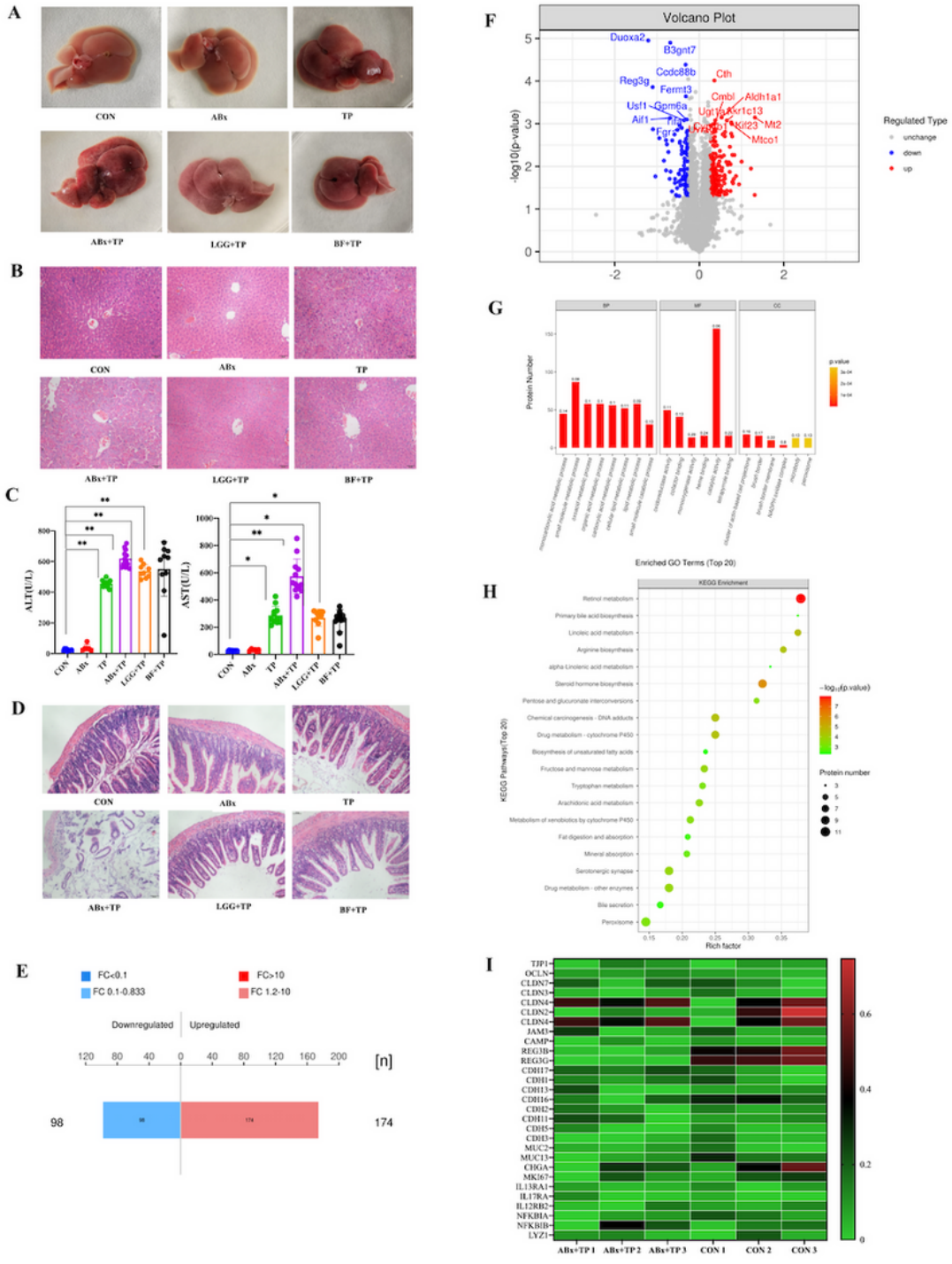


Figure 4

(A) External view of liver tissue. (B) Histological examination of liver tissue. (C) AST and ALT levels of serum. (D) Histological examination of ileum tissue. (E) Histogram of protein quantitative results. (F) Volcano diagram of differential proteins between the CON *vs.* ABx+TP Groups. (G) GO annotation statistics of differentially abundant proteins between the CON and ABx+TP groups (top 20). (H)

Enrichment bubble diagram of KEGG pathways between the CON and ABx+TP groups. (I) Heatmap of intestinal barrier-associated proteins.

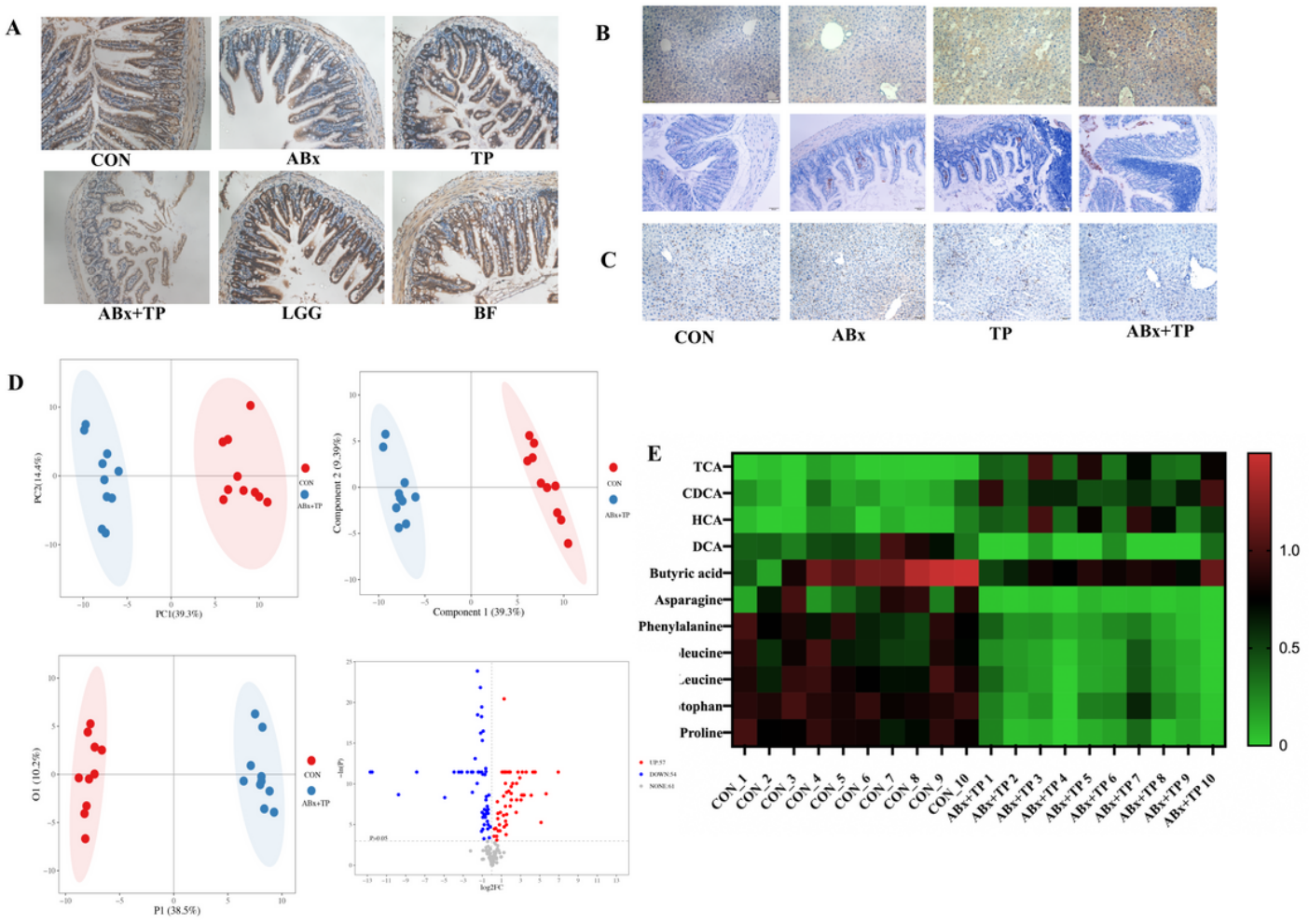


Figure 5

(A) Expression of REG3G in ileum tissue. (B) Expression of NLRP3+ inflammatory bodies in liver and ileum tissue. (C) Expression of F4/80 in liver tissue. (D) PCA score map, PLS-DA score map, OPLS-DA score map, and univariate metabolite volcano map of the CON vs ABx+TP group. (E) Heatmap of differential metabolites in liver between the CON and ABx+TP groups.

Supplementary Files

This is a list of supplementary files associated with this preprint. Click to download.

- SupplementalInformation.docx
- GraphicalAbstract.png